DigiMon Deliverable D2.7: Project report and algorithms for optimizing acquisition layout and frequency

Digital monitoring of CO$_2$ storage projects

Prepared by

Robert Mellors[a,b], Arben Pitarka[b], Joshua White[b], and Martha Lien[c]

[a] Scripps Institute of Oceanography, University of California, San Diego, CA, USA

[b] Lawrence Livermore National Laboratory, Livermore, CA, USA

[c] OCTIO Environmental Monitoring AS, Bergen, Norway

Scope

D2.7. Project report and algorithms for optimizing acquisition layout and frequency

We evaluate the capability of 3D finite difference codes to model Distributed Acoustic Sensors (DAS) at reservoir scale for monitoring of CO_2 sequestration. This work builds on previous DigiMon deliverables: 1.3 - DAS synthetic dataset (Baird et al, 2020b) and 2.1 - Framework for forward modelling of the DigiMon data (Vandeweijer et al, 2021). The goals of this work include 1) evaluation of the computational load and trade-offs needed to model Distributed Acoustic Sensing (DAS) signals from a 3D (~14x14x3 km) model of a CO_2 sequestration reservoir; 2) sensitivity of various DAS deployment models (borehole versus surface); 3) comparison of DAS (linear and helical) with respect to geophones for both vertical and surface installations; and 4) measurements of possible induced seismicity with DAS.

Revision

Version	Date	Change	Page
1.0	11/1/2022	Draft version	All
1.1	11/21/22	Check of document and minor updates of text and spelling.	All
1.2		Update after review	

Document distribution

ACT Coordinator

- Research Council of Norway

ACT national funding agencies

- Forschungszentrum Jülich GmbH, Projektträger Jülich, (FZJ/PtJ), Germany.
- Geniki Grammatia Erevnas kai Technologias/The General Secretariat for Research and Technology (GSRT), Greece.
- Ministry of Economic Affairs and Climate/Rijksdienst voor Ondernemend Nederland (RVO), the Netherlands.
- The Research Council of Norway (RCN), Norway.
- Gassnova, Norway.
- Development and Executive Agency for Higher Education, Research, Development and Innovation Funding (UEFISCDI), Romania.
- Department for Business, Energy and Industrial Strategy (BEIS), UK.
- Department of Energy (DoE), USA.

DigiMon partners

- NORCE Norwegian Research Centre AS
- OCTIO Environmental Monitoring AS
- NTNU Norwegian University of Science and Technology
- University of Bristol
- University of Oxford
- CRES Centre for Renewable Energy Sources and Saving
- Helmholtz–Centre for Environmental Research
- Sedona Development SRL
- TNO Nederlandse Organisatie voor toegepast -natuurwetenschappelijk Onderzoek
- Geotomographie GmbH
- LLC Lawrence Livermore National Security
- SILIXA LTD
- EQUINOR ASA
- REPSOL –NORGE AS

Table of contents

1 Background

Carbon capture and storage (CCS) is a key component of most strategies for reducing greenhouse gases in the atmosphere. The overall objective of the DigiMon project is to "develop and demonstrate an affordable and smart Digital Monitoring early-warning system" for monitoring subsea CO_2 storage reservoirs. One focus is distributed fiber-optic sensing, as fiber-optic sensors may be a low-cost and robust method of monitoring subsea reservoirs. Here we explore preferred geometries for DAS acquisition layout (vertical borehole versus horizontal surface) and compare, using synthetics, the expected performance of DAS and standard geophones for monitoring the reservoir and possible induced seismicity. We use a large-scale 3D model to allow for 3D variations.
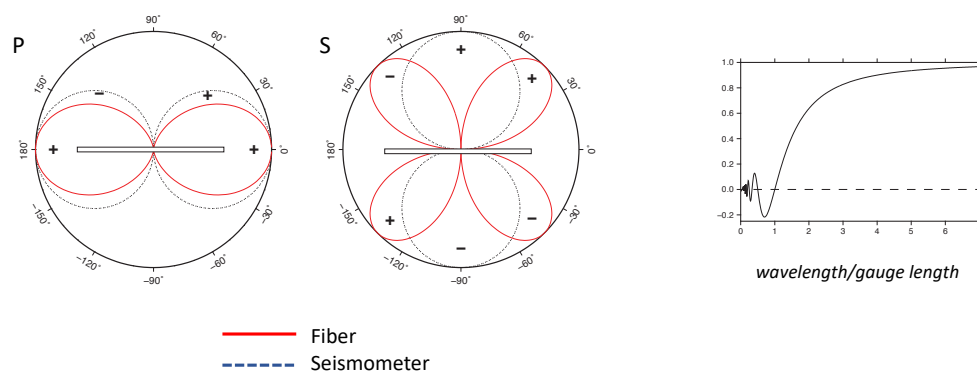

Figure 1.1 (left) Response of linear DAS fiber (e.g., strainmeter) compared with a geophone. (right) Wavelength/gauge length response.

DAS sensors measure strain along discrete lengths of fiber as a function of distance (Hartog,2017). In comparison, geophones measure velocity at a point. While the two measurements are related, significant differences exist (e.g., Martin, 2018). Strain is a tensor field rather than a vector field, and the longitudinal azimuthal (a) response is $cos^2(a)$, while the transverse azimuthal (a) response is $sin(a)cos(a)$. The frequency response is essentially flat for wavelength >> gauge length (1-10 m) (Figure 1.1).

This work builds on previous deliverables. Baird et al. (2020b) focused on modeling DAS using standard seismic modelling codes. A selection of three codes was tested for use in creating DAS synthetics: a spectral element code (SPECFEM), a finite difference (SW4), and a semi-analytic code (Chapman, 2004). The model was a 3D (3x3x3 km) volume with a layered velocity model. All three yielded similar results with some differences in implementation (model complexity, receiver spacing, particle motion output, boundary conditions). Vandeweijer et al. (2021) investigated using DAS/seismic synthetics as part of an inversion toolkit with multiple geophysical tools. A 2D rather than a spectral element synthetic code was used due to constraints on speed required for inversion. The goal of the inversion was to resolve changes in reservoir due to injection (Bhakta et al., 2022).

In this work, we evaluate capability of a 3D finite difference code to model Distributed Acoustic Sensors (DAS) at (near) reservoir scale for monitoring of CO_2 sequestration. Reservoir scale is assumed to be on

the order of 10-20 km, or more, in horizontal extent. We focus on the following questions, which can reasonably addressed by numerical modelling.

- How many processors and time are required to conduct 3D models, and what are the technical limits/trade-offs? (e.g., frequency, geometry). This is important both for forward modeling and inversion. Inversion typically requires multiple forward models and hence it is important to understand the speed and accuracy of forward models.
- How can changes due to CO_2 injection be measured over time for difference fiber deployment geometries: DAS in vertical borehole versus horizontal (seafloor)? Monitoring the CO2 injection is essential for understanding effects on the reservoir and any potential leaks. The monitoring must be effective in terms of both resolution and cost.
- How does DAS (both linear and helical) compare to geophones for possible acquisition layouts? While DAS possess considerable potential for long-term monitoring, it is important to understand with respect to a highly-mature and well-tested technology such as geophones.
- How well can DAS resolve possible induced seismic events? Induced seismicity is a potential side effect and it is important to understand how well it can be monitored both for magnitude, location, and focal mechanism.

Method

1.1 Modelling

The modelling used SW4, a 3D finite difference code to simulate changes in a 3D model caused by the injection of CO_2 into a brine reservoir at depth.
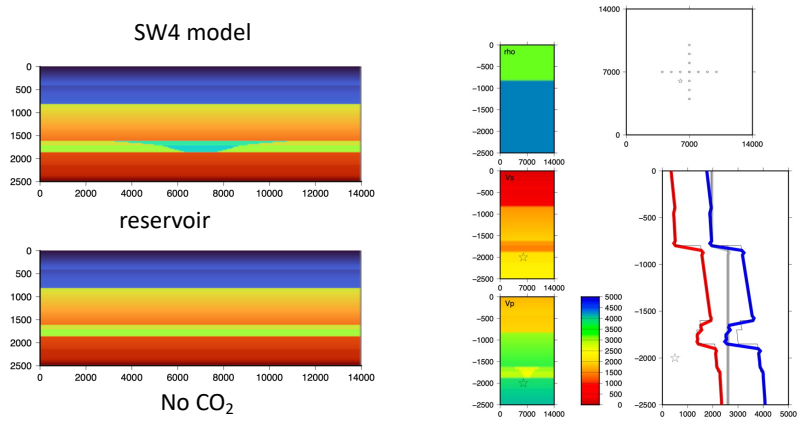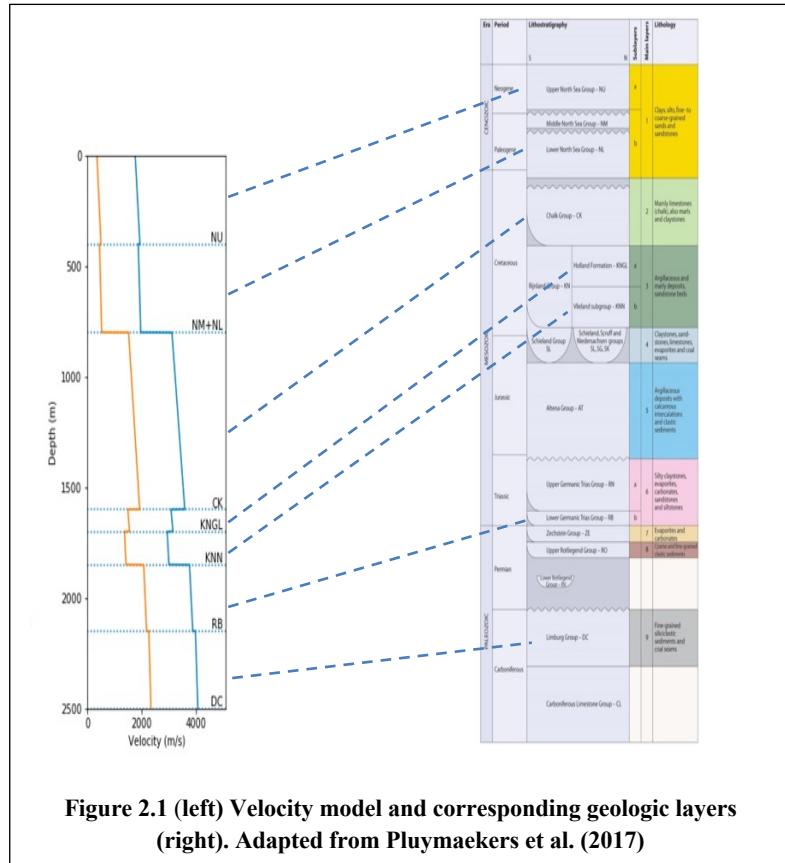
1.1.1 Codes

The code (SW4) is an open-source, node-based 4th order 3D finite difference code that is widely used for modelling seismic waveforms (Petersson and Sjogreen, 2018) and has been fully tested on massively parallel machines and scales up to 'exascale' capability on 1,000's of compute nodes (Sjogreen, 2018; Rodgers et al., 2019). Features include the capability to handle an irregular surface, mesh refinement, and absorbing boundary conditions. One specific output is the full strain tensor, which is useful for modelling DAS strain waveforms. Disadvantages of SW4 include the inability to model a water layer and that output can only be generated at a node location. We have extensive experience with SW4 and, although other alternate choices exist (e.g., SPECFEM; Komatitsch and Tromp, 1999), we chose to use SW4 for ease of use. The code was run both on massively parallel machines at LLNL and smaller (8-node) machines at UCSD.

1.1.2 Velocity model

We use the same model as was used in Deliverable 1.3 (Baird et al, 2020b). It is a 1D based on the publicly available VELMOD-3 (Dutch North Sea) model (Pluymaekers et al., 2017) that was adapted by Baird et al. (2020) to include S wave velocities based on Costagna et al., (1985) and an ad hoc density model (Figure 2.1)

1.1.3 CO_2 injection

We assume an 'ad hoc' adaptation of the model to simulate the injection of CO_2 into a brine aquifer in one layer (early Cretaceous sandstone beds overlain by a thick chalk layer). Sufficient CO_2 is assumed to have been injected to form an inverted cone of CO_2 within the reservoir (Figure 2.2) as has been observed elsewhere (Celia et al.,2015).

Figure 2.1 (left) Velocity model and corresponding geologic layers (right). Adapted from Pluymaekers et al. (2017)

Figure 2.2 Graphical representation of the SW4 model with CO2 injection (top left) and without (bottom left). Images on right show the surface receiver layout and P (blue) and S (red) velocity model versus depth. Color lines indicate power-injection and black is pre-injection. Gray line is density.

The injection is sufficient to produce up to approximately 30% saturation with a corresponding change in P velocity of 15% (Landro and Zumberge, 2016). For this initial study, changes in density due to the CO_2 plume (Celia et al., 2015) is not included to isolate the effect of changes in Vp on the seismic response. No change in S velocity is assumed (Vasco et al., 2019; Guitierrez et al., 2020). It is unclear how valid these assumptions are, but as we focus on P waves for this work, changes in S waves should not have major impact on the results presented here. We do not assume a change in attenuation or changes in effective stress. The observational strategy is to conduct time-lapse surveys before ($NoCO^2$) and after (CO_2) injection.

1.1.4 Induced events

It has been observed that some CO_2 injections produce induced seismicity. In some areas (Insalah), the seismicity occurs in the cap rock (Stork et al., 2015), while in others (Decatur)(Kaven et al., 2014), the events occur at reservoir depth and deeper. Here we assume events below the reservoir as the chalk cap rock above the reservoir may deform aseismically.

1.2 Effect of deployment geometry

It is expected that the DAS response, unlike geophones, will vary with the angle of the fiber with respect to the incoming wave. We simulate the expected performance of DAS on various possible acquisition layouts for both induced seismicity at depth and for a surface seismic source such as those used in seismic reflection and time-lapse surveys.

1.2.1 Sensor geometry for imaging induced seismicity

For a deep source, such as an in induced event, we test two observation deployments: a vertical borehole and a horizontal deployment. We want to evaluate which is more effective. A secondary goal is to see if microseismic signals can be used as a source to measure changes in the reservoir. We also want to evaluate model size versus computation time and frequency. The source is a double couple with a magnitude of approximately 2.

1.2.2 Sensor geometry for seismic reflection

Similar tests are repeated for a surface source to mimic a seafloor reflection survey. For full resolution we would need to test a series of shots to mimic a full reflection survey, but we restrict ourselves here to a single source. If differences can be observed for a single source, then we are confident that a complete survey will be effective. As above, we evaluate a surface array and a vertical borehole. The simulated "surface" source is a Ricker wave.

1.2.3 Helical fiber

One difficulty with fibre sensors is that sensitivity to OP waves is poor when the waves arrive perpendicular to the fibre, as occurs with seismic reflection surveys. One way to alleviate this effect is to wind the fibre in a helix around the cable (Figure 2.4) . Depending on the winding angle, this will increase the sensitivity to P waves at near a 90 degree angle (Baird et al., 2020a).
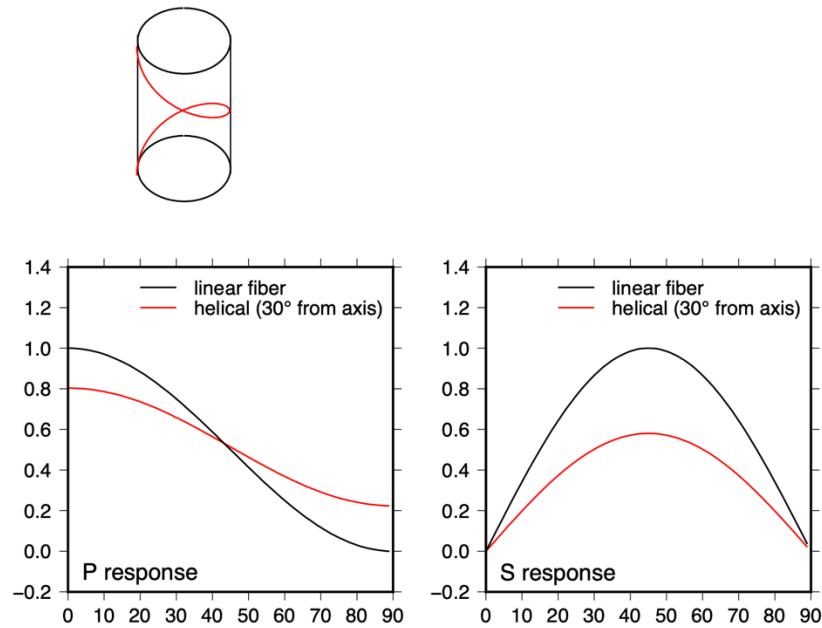
Figure 2.4 P and S response of linear (black) and helical fibre (red) for a winding angle of 30 degrees (measured from axis).

2 Results

2.1 Modelling

2.1.1 Large reservoir model.

The full model was 14x14x3 km with a grid spacing of 12 m and an upper frequency of 40 Hz. This required approximately 4 hours of wall clock time and 2304 CPU (64 nodes at 36 CPU/node). 12 m is slightly longer than the standard gauge length for DAS (usually 2 – 10 m) but is adequate for this work. The assumption is that each DAS channel represents an average over the gauge length.

The initial test assumed a double-couple source at a depth of 2500 m, which is below the reservoir and represents a possible induced seismic source. Simulations were conducted on models representing both before and after a CO_2 injection sequence to investigate whether changes in DAS waveforms are evident. For actual induced events, the exact timing and location would not be known precisely, but differences are apparent in relative phase timing and amplitude for the waveforms, which suggest that a systematic change might be observable (Figure 3.1).
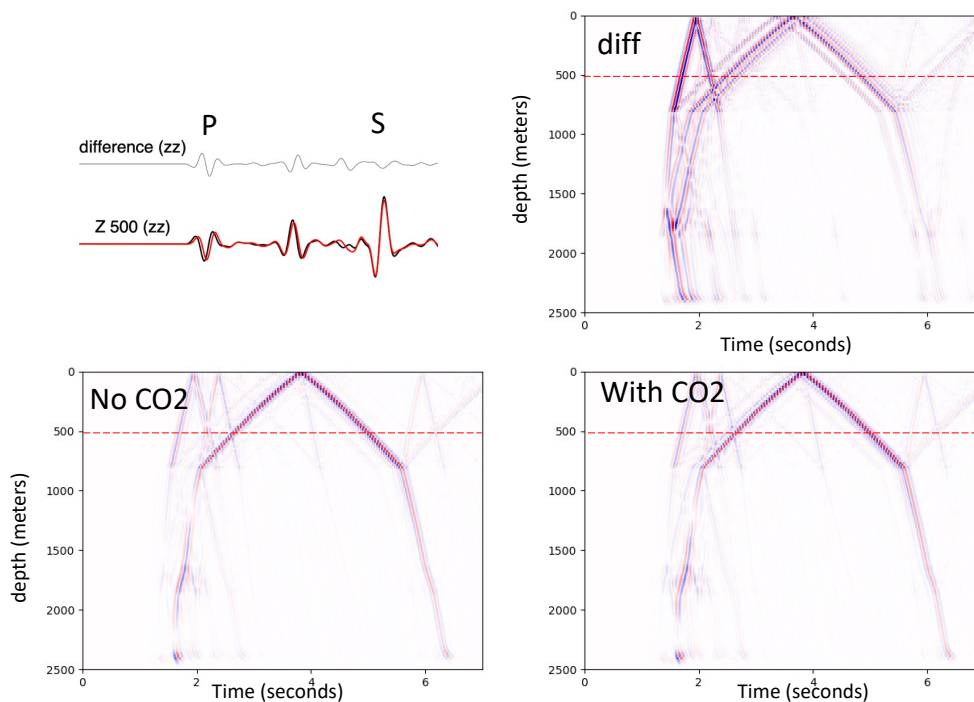
Figure 3.1. Images (vertical cross-sections) of the pre-injection and post-injection waveforms from a simulated induced earthquake below the reservoir as recorded on a vertical DAS installed in a borehole that extends to reservoir depth.

2.1.2 Focused small-scale models

Small-scale models were used to compare differences between vertical DAS and geophones, as a variety of tests could be made quickly using these models. The first set examined measurements of a surface source on vertical DAS and geophones, with emphasis on reflected phases that would be sensitive to changes in the reservoir caused by injection. For the vertical borehole, both DAS and geophones resolved the signals and changes caused by velocity changes due to the CO_2 injection. The changes were in both amplitude and phase and were more obvious at reservoir level but also on the reflected phases above. We conclude that the vertical DAS appears to be as effective as the geophones (assuming similar sensitivity) (Figures 3.2 and 3.3).
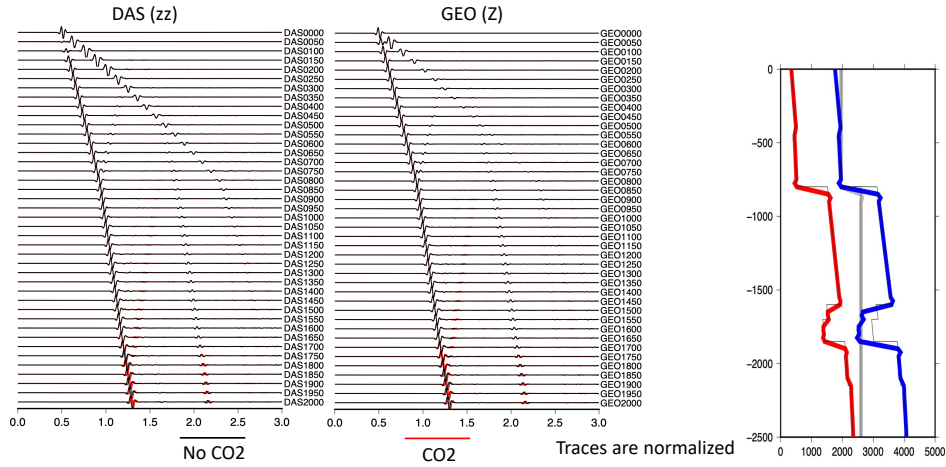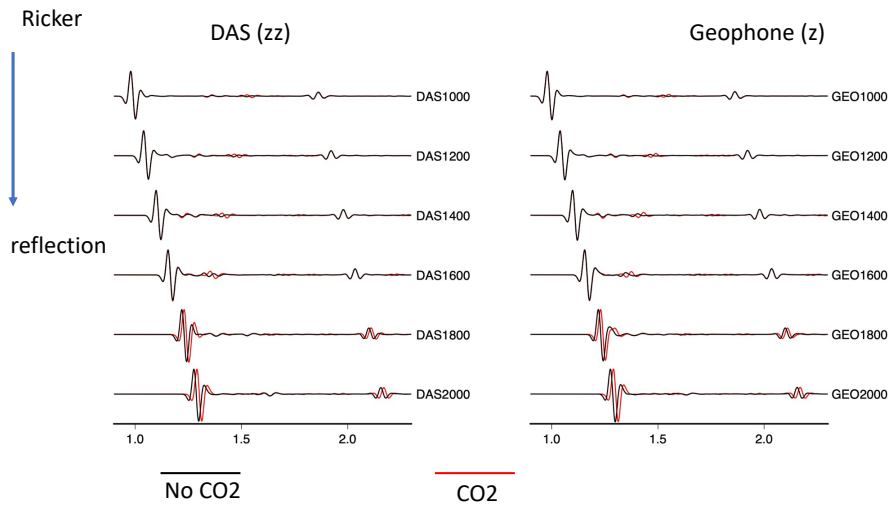
Figure 3.2. Comparison of DAS (vertical fiber) and geophone (Z) for a surface source. Red is post-injection and black id pre-injection.

Figure 3.3. Enhanced view of the pre- and post-injection waveforms demonstrating that differences in phase and amplitude are evident on both DAS and geophone.
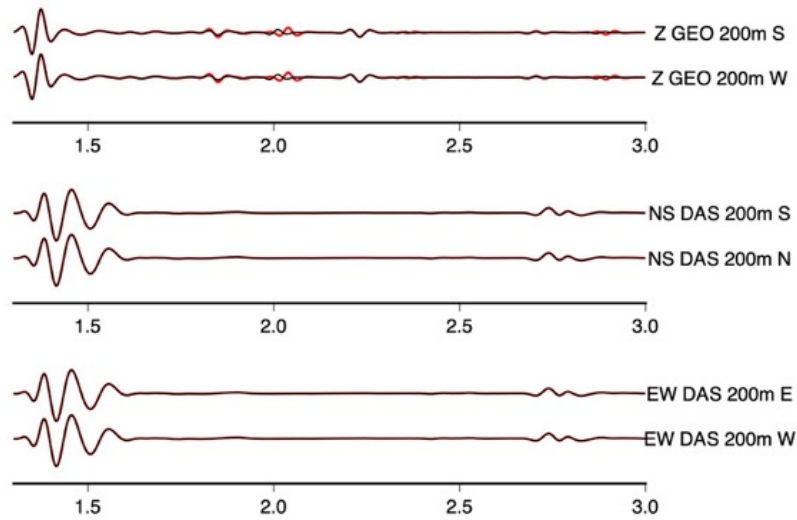
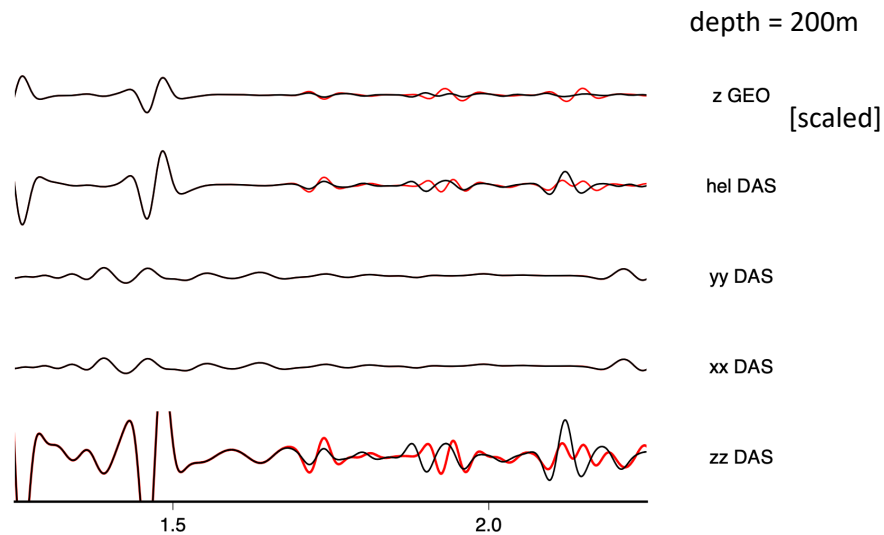**Figure 3.4. Pre- and post-injection waveforms from surface DAS (EW and NS lines) and geophones.**

Figure 3.5. Pre- and post-injection waveforms from surface helical (hel) DAS (EW and NS lines) compared with linear DAS (xx, yy and zz) directions.

Next, we examined the difference between surface DAS and surface geophones. One difficulty is that the SW4 code boundary conditions force the vertical strain to go to zero at the surface, so we use a depth of 200 m to avoid boundary condition effects. As expected, DAS sensitivity to reflected near-vertical P waves is poor and the geophones (Z) performance is better.

One possible way to improve the performance of DAS to perpendicular arrivals is through the use of helical fibre.

3 Conclusion and recommendations

We find that a 3D elastic model of a reservoir that is 14x14x3 km with a grid spacing of 12 m and an upper frequency of 40 Hz is sufficient to model the expected frequencies and observations of DAS. This model required approximately 4 hours of wall clock time while running on 2304 CPU (64 nodes at 36 CPU/node).

Changes in the reservoir due to CO_2 injection cause changes in both the reflected and tranmitted seismic waves from surface sources. These changes occur both in amplitude and phase. DAS installed in a vertical monitoring well is more sensitive than than DAS on a horizontal surface cable. This is due in part to the increased longitudinal sensitivity of DAS to compressional waves as well as proximity to the reservoir.

Comparisons between the modelled response for DAS and geophones suggested that the expected sensitivity (ignoring instrument self-noise) is comparable for the vertical borehole but that horiozontal DAS cables on the surface are less sensitive than geophones. The use of helical DAS fibre appears to show a slight improvement but we are still evaluating the validity of numerical approximation near the surface. Simulations of induced events are also recorded better on vertical monitoring wells than the surface for DAS.

Reccomendations for future work include:

- Coupling of a reservoir model to the elastic to provide a more accurate simulation of the changes and to assess resolution. This is particarly critical for calibrating changes in saturation.
- A more comprehensive understansing of the effect of reservoir changes on S wave amplitudes.
- Comparisons with data from ongoing CO_2 sequestration projects in similar geology and focused DAS testbeds. The goal is to understand and model the DAS response and coupling to achieve accuracies comparable with standard seismic sensors.
- Verifying these results with other code to ensure that the water layer, which has not been included in these models due to limitations in SW4, does not significantly influence the results.

4 Acknowledgements

5 References

Baird A., Modelling the Response of Helically Wound DAS Cables to Microseismic Arrivals, 2020a, Conference Proceedings, First EAGE Workshop on Fibre Optic Sensing, Mar 2020, Volume 2020, p.1-5

Baird, A., R. Mellors, B. Paap, V. Vandeweijerc, A. Verdel, A. Butcher, and A. L. Stork, 2020s, Deliverable 1.3: DAS synthetic dataset, DigiMon Deliverable D.1.3 Version 1.2, August 2020.

Bhakta, T., B. Paap, V Vandeweijer, and T. Mannseth, 2022, Monitoring of CO2 plume movement using time-lapse distributed acoustic sensing (DAS) data. Conference: Second International Meeting for Applied Geoscience & Energy, 478-482. 10.1190/image2022-3745759.1

Castagna, J.P., Batzle, M.L. & Eastwood, R.L., 1985, Relationships between compressional-wave and shear-wave velocities in clastic silicate rocks. Geophysics, 50, 571–581, 1985.

Celia, M. A., S. Bachu, J. M. Nordbotten,and K. W. Bandilla, 2015, Status of CO2storage in deep saline aquifers with emphasis on modeling approaches and practical simulations, WaterResour. Res.,51, 6846–6892,doi:10.1002/2015WR017609.

Chapman, C., 2004, Fundamentals of Seismic Wave Propagation, Cambridge University Press, 608 pages.

Eigestad, G.T., Dahle, H.K., Hellevang, B., Riis, F., Johansen, W.T., Øian, E., 2009. Geological modeling and simulation of CO 2 injection in the Johansen formation. Comput. Geosci. 13 (4), 435.

Guitierrez, M., D. Katsuke, and A. Almrabat, 2020, Seismic velocity change in sandstone during CO2 injection,ICEGT,2020,https://doi.org/10.1051/e3sconf/202020502001

Hartog, A. H., 2017, An Introduction to Distributed Optical Fibre Sensors, CRC Press, 472 pages, https://doi.org/10.1201/9781315119014.

Kaven, J. O., S. H. Hickman, A. F. McGarr, S. Walter, W. L. Ellsworth, 2014, Seismic monitoring at the Decatur, IL, CO2 sequestration demonstration site, Energy Procedia, Vol. 63, 4264-4272, ISSN 1876-6102, https://doi.org/10.1016/j.egypro.2014.11.461.

Komatitsch, D., and Tromp, J. 1999, Introduction to the spectral element method for three-dimensional seismic wave propagation. Geophysical journal international 139, 3, 806–822.

Landrø M., Zumberge M., 2016, Estimating saturation and density changes caused by CO2 injection at Sleipner — Using time-lapse seismic amplitude-variation-with-offset and time-lapse gravity, SEG Interpretation, Volume 5, Issue 2, May 2017, Pages: 1M-T277

Martin, E., 2018, Passive Imaging and Characterization of the Subsurface with Distributed Acoustic Sensing, Ph.D thesis, Stanford University, 185 pages.

Petersson, N. A., and Sjögreen, B. 2018, High order accurate finite difference modeling of seismo-acoustic wave propagation in a moving atmosphere and a heterogeneous earth model coupled across a realistic topography. Journal of Scientific Computing 74, 1, 290–323.

Pluymaekers, M. P. D., Doornenbal, J. C., and Middelburg, H., 2017, Velmod-3.1. Tech. Rep. R11014, TNO. Available at https://www.nlog.nl/sites/default/files/060.26839%20r11014%20doornenbal-final.sec.pdf

Rodgers, A., N. A. Petersson, A. Pitarka, D. B. McCallen, B. Sjogreen, and N. Abrahamson, 2019, Broadband (0–5 Hz) Fully Deterministic 3D Ground-Motion Simulations of a Magnitude 7.0 Hayward Fault Earthquake: Comparison with Empirical Ground-Motion Models and 3D Path and Site Effects from Source Normalized Intensities. Seis. Res. Lets 2019; 90 (3): 1268–1284. doi: https://doi.org/10.1785/0220180261

Sjögreen, B., 2018, SW4 final report for iCOE, LLNL-TR-759417, available at https://www.osti.gov

Stork, A. L., J. P. Verdon, and J. M. Kendall, 2015, The microseismic response at the In Salah Carbon Capture and Storage (CCS) site, International Journal of Greenhouse Gas Control, Vol. 32,159-171, https://doi.org/10.1016/j.ijggc.2014.11.014.

Vandeweijer, V., B. Paap, T. Candela, T. Bhakta, and M Lien, 2021, DigiMon Deliverable D.2.1 Version 2.1, June 2021.

Vasco, D. W., Alfi, M., Hosseini, S. A., Zhang, R., Daley, T., Ajo-Franklin, J. B., & Hovorka, S. D. (2019). The seismic response to injected carbon dioxide: Comparing observations to estimates based upon fluid flow modeling. Jour. Geophys. Res.: Solid Earth, 124, 6880– 6907. https://doi.org/10.1029/2018JB016429

6 Appendix B: SW4 input files

6.1.1 Example partial input file.

In this example, black denotes comments, green is input and red denotes input that has been commented out but could be used. This particular file uses a 'pfile' for specifying a 3D velocity model. The file also includes a 'block' representation (commented out) that could be used instead of a pfile for this model.

```
# simple grid
grid h=5 x=14000 y=14000 z=2500
#refinement zmax=2100
#
source x=6000 y=6000 z=2000 t0=3.0  type=Gaussian freq=20.0 m0=1e12 strike=110 dip=73 rake=20
#
#fileio path=NorthSea_14x14_CO2.h50
```

```
#pfile style=cartesian filename=NorthSea_14x14_CO2.ppmod
#
fileio path=NorthSea_14x14_NoCO2.h50
pfile style=cartesian filename=NorthSea_14x14_NoCO2.ppmod
#
time t=6.0 utcstart=08/24/2020:00:00:00.00
#
#
##block vp=1761.00 vpgrad=0.44 vs=345.69 vsgrad=0.38  rho=1960.00 z1=0.00
##block vp=1779.00 vpgrad=0.23 vs=361.21 vsgrad=0.20  rho=1960.00 z1=400.00
##block vp=2646.00 vpgrad=0.59 vs=1108.62 vsgrad=0.51 rho=2600.00 z1=800.00
##block vp=1907.00 vpgrad=0.74 vs=471.55 vsgrad=0.64  rho=2600.00 z1=1600.00
##block vp=2217.00 vpgrad=0.43 vs=738.79 vsgrad=0.37  rho=2600.00 z1=1700.00
##block vp=3019.00 vpgrad=0.41 vs=1430.17 vsgrad=0.35 rho=2600.00 z1=1850.00
##block vp=3427.00 vpgrad=0.26 vs=1781.90 vsgrad=0.23 rho=2600.00 z1=2150.00
#
# Velocity image output
#
image mode=p x=7000 file=imageVP cycle=1
image mode=s x=7000 file=imageVS cycle=1
image mode=rho x=7000 file=imageRHO cycle=1
#
#
# image vertical wavefield
image mode=uz x=7000 file=image_uz cycle=100
#
# receiver output
# depth
#
sac x=7000 y=7000 z=0 sta=Z0000 file=Z0000 variables=velocity nsew=1
sac x=7000 y=7000 z=0 sta=Z0000 file=Z0000 variables=strains  nsew=1
sac x=7000 y=7000 z=20 sta=Z0020 file=Z0020 variables=velocity nsew=1
sac x=7000 y=7000 z=20 sta=Z0020 file=Z0020 variables=strains  nsew=1
sac x=7000 y=7000 z=40 sta=Z0040 file=Z0040 variables=velocity nsew=1
sac x=7000 y=7000 z=40 sta=Z0040 file=Z0040 variables=strains  nsew=1
sac x=7000 y=7000 z=60 sta=Z0060 file=Z0060 variables=velocity nsew=1
```

6.1.2   Example partial pfile.

Top of 'pfile' used in the above example.
Name: 'NorthSea_14x14_NoCO2.ppmod')

NorthSea
100
140 0 14000
140 0 14000
100 0 2500
-99 -99 -99 -99
.FALSE.
0 0 100
1 0 1761.00 345.69 1960.00
2 25 1772.00 355.19 1960.00
3 50 1783.00 364.69 1960.00
4 75 1794.00 374.19 1960.00
5 100 1805.00 383.69 1960.00
6 125 1816.00 393.19 1960.00
7 150 1827.00 402.69 1960.00
8 175 1838.00 412.19 1960.00
9 200 1849.00 421.69 1960.00
10 225 1860.00 431.19 1960.00
11 250 1871.00 440.69 1960.00
12 275 1882.00 450.19 1960.00
13 300 1893.00 459.69 1960.00
14 325 1904.00 469.19 1960.00
15 350 1915.00 478.69 1960.00
16 375 1926.00 488.19 1960.00
17 400 1937.00 497.69 1960.00
18 425 1876.75 446.21 1960.00